Soft Matter

Development of the Computational Antibiotic Screening Platform (CLASP) to Aid in the Discovery of New Antibiotics

Journal:	*Soft Matter*
Manuscript ID	SM-ART-11-2020-002035.R1
Article Type:	Paper
Date Submitted by the Author:	01-Jan-2021

Complete List of Authors:	Dai, Yinghui; Syracuse University, Department of Biomedical and Chemical Engineering Ma, Huilin ; Syracuse University, Wu, Meishan; Syracuse University, Department of Biomedical and Chemical Engineering Welsch, Tory; Syracuse University, Department of Biomedical and Chemical Engineering Vora, Soor; Syracuse University, Department of Biomedical and Chemical Engineering Ren, Dacheng; Syracuse University, Biomedical and Chemical Engineering Nangia, Shikha; Syracuse University, Department of Biomedical and Chemical Engineering

Development of the Computational Antibiotic Screening Platform (CLASP) to Aid in the Discovery of New Antibiotics

Yinghui Dai†, Huilin Ma†, Meishan Wu, Tory Alane Welsch, Soor Rajiv Vora, Dacheng Ren, and Shikha Nangia*

Department of Biomedical and Chemical Engineering, Syracuse University, Syracuse, NY 13244, USA

Abstract: Bacterial colonization of biotic and abiotic surfaces and antibiotic resistance are grand challenges with paramount societal impacts. However, in the face of increasing bacterial resistance to all known antibiotics, efforts to discover new classes of antibiotics have languished, creating an urgent need to accelerate the antibiotic discovery pipeline. A major deterrent in the discovering of new antibiotics is the limited permeability of molecules across the bacterial envelope. Notably, the Gram-negative bacteria have nutrient specific protein channels (or porins) that restrict the permeability of non-essential molecules, including antibiotics. Here, we have developed the ComputationaL Antibiotic Screening Platform (CLASP) for screening of potential drug molecules through the porins. The CLASP takes advantage of coarse grain (CG) resolution, advanced sampling techniques, and a parallel computing environment to maximize its performance. The CLASP yields comprehensive thermodynamic and kinetic output data of a potential drug molecule within a few hours of wall-clock time. Its output includes the potential of mean force profile, energy barrier, the rate constant, and contact analysis of the molecule with the pore-lining residues, and the orientational analysis of the molecule in the porin channel. In our first CLASP application, we report the transport properties of six carbapenem antibiotics—biapenem, doripenem, ertapenem, imipenem, meropenem, and panipenem—through OccD3, a major channel for carbapenem uptake in *Pseudomonas aeruginosa*. The CLASP is designed to screen small molecule libraries with a fast turnaround time to yield structure-property relationships to discover antibiotics with high permeability. The CLASP will be freely distributed to enable accelerated antibiotic drug discovery.

†contributed equally

*Address for correspondence:
Dr. Shikha Nangia
343 Link Hall
Department of Biomedical and Chemical Engineering
Syracuse University, Syracuse, NY 13244, USA
Phone (315) 443 0571 | Email: snangia@syr.edu

1. INTRODUCTION

Antibiotic resistant bacteria are endangering the efficacy of known antibiotics, which have saved millions of lives since the middle of the last century.[1-4] In the past few decades, antibiotics have become the most prescribed drugs in human medicine. However, over prescription and misuse of antibiotics have led to the upsurge in bacterial resistance.[5] To make matters worse, the drug discovery pipeline is at a virtual standstill due to limited profits and regulatory bottlenecks.[6] The development of a new antibiotic is a prolonged process requiring years of drug screening, *in vitro* testing, clinical trials, and billions of dollars in investment. Therefore, there is an urgent need to accelerate the screening of drug candidates and develop new antibiotics.[7-10]

A bottleneck in a drug molecule's penetration into a bacterial cell is the multilayered bacterial envelope.[11] Both Gram-positive and Gram-negative bacteria have evolved a sophisticated and complex cell wall that protects them from hostile chemical environments. For Gram-negative bacteria in particular, their liposaccharide-rich, negatively charged outer membranes with narrow, water-filled protein channels (or porins) allow selective uptake of nutrients, while preventing the passage of toxins into the cell.[12-13] The chemical nature (lipophilic versus hydrophilic) of the antibiotic molecule determines whether the permeation occurs via the lipid-mediated or the porin-mediated pathway.[13]

A critical step in antibiotic discovery is to identify chemical compounds with high permeability through Gram-negative bacterial outer membranes. The bacterial outer membrane porins are passive transporters of water-soluble molecules with a size limit of 600-700 Da.[13 ,14-15] Besides mediating uptake of nutrients for survival, porins fortuitously allow the diffusion of antibiotics across the outer membrane.[16-17] For example, β-lactams, including cephalosporins, penicillins, and carbapenems, are known to penetrate the outer membrane through the porins.[11] These small molecule portals make the bacteria more susceptible to new classes of antibiotics.

Understanding the porin-mediated uptake of small molecules at a molecular-level can spur the identification of natural compounds or aid in the rational design of new classes of antibiotics. Screening for penetration experimentally is challenging due to the low-throughput nature of related procedures. The use of computational approaches can provide molecular insights that are undetectable via currently available experimental methods.[18-24] For example, advanced simulation approaches, such as metadynamics,[20,25-26] steered molecular dynamics,[19,21] umbrella sampling,[27-28] and accelerated molecular dynamics simulations[29] have been used to simulate translocation through bacterial porins. However, these and other computational methods do not provide high-throughput thermodynamic and kinetic data of uptake of substrate molecules, precluding the high-throughput screening of libraries of natural compounds as possible antibiotics.

To advance screening of molecular libraries for the identification of potential antibiotics, in this work, we report the development of the Computational Antibiotic Screening Platform (CLASP). The CLASP takes advantage of coarse-grained (CG) resolution, advanced sampling techniques, and a parallel computing environment to maximize performance. The CLASP yields comprehensive thermodynamic and kinetic data of a solute's transport through a bacterial outer membrane porin. Its output includes the potential of mean force profile, energy barrier, rate constant of the molecule's transport, contact analysis of the molecule with the pore-lining residues, and the orientational analysis of the molecule in the porin channel. The CLASP automated workflow yields result in less than two hours of wall-clock time. The output turnaround times can be further improved with an increase in computer resources.

Our first CLASP application focuses on antibiotic uptake by *Pseudomonas aeruginosa*, a multi-drug resistant Gram-negative bacterium. Compared to other common Gram-negative bacterial species, the membrane permeability of *P. aeruginosa* is about one order of magnitude lower, primarily due to the presence of substrate-specific porins with sub-nanometer diameters.[30-31] As a result, the development of new drugs to treat infections caused by *P. aeruginosa* has been a major challenge.[10] In the 2019 Antibiotic Resistance report, published by the Centers for Disease Control and Prevention, *P. aeruginosa* was identified as a serious threat for infections in the United States.[32]

Among the *P. aeruginosa* porins, the most important is the Outer membrane Carboxylate Channel (Occ) family that are dedicated to the uptake of small, water-soluble, carboxylate containing solutes. In recent years, several members of the Occ family have been studied, including OccD1 and OccD3 that facilitate permeation of arginine, dipeptides, and carbapenem antibiotics.[33-34] As the first member of the Occ family, OccD1 porin has been studied extensively via experimental[22,35-38] and computational[19-21] approaches. The closely related OccD1 ortholog, OccD3 has also been implicated as a channel for carbapenem uptake.[33-34,39] We focused our investigation on OccD3, which has high structural similarity and higher ion conductance than OccD1.[34] The OccD3 is a β-barrel porin formed by 18 β-strands that are connected by large extracellular loops and short turns.[39] The porin's lumen is hourglass-shaped, which has a 3.7 Å diameter bottleneck region (Figure 1).

We investigated six members of the carbapenem family of antibiotics—biapenem, doripenem, ertapenem, imipenem, meropenem, and panipenem. The carbapenem family is one of the limited classes of antibiotics that can treat *P. aeruginosa* infections.[40-44] The carbapenems are effective because they have a lower propensity to enzymatic degradation inside the bacterial cell, and are therefore, commonly prescribed for the treatment of infections caused by *P. aeruginosa*.[44] Understanding the mechanism of carbapenems' transport and is imperative to develop new drugs and reduce the threat of *P. aeruginosa*.

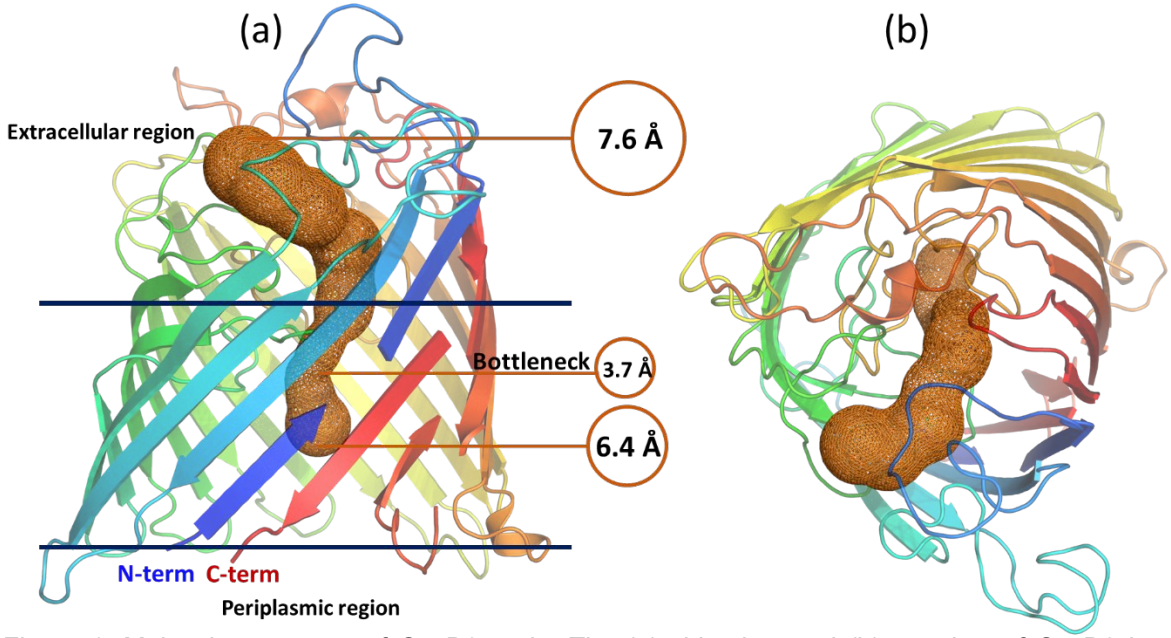

Figure 1. Molecular structure of OccD3 porin. The (a) side-view and (b) top-view of OccD3 in cartoon representation (colored blue to red from N-term to C-term) along with the porin channel (in orange surface representation). The diameter of the channel is marked in circles. The two horizontal lines show the membrane embedded region of the porin.

The results provide the details of the CLASP application and comprehensive analysis of the translocation profiles of the six carbapenems through OccD3. The free energy profiles and the energy barriers for carbapenem translocation are consistent with previous reports in the literature. Besides, we computed the contact frequencies between the carbapenem molecules and each OccD3 protein residue, which identified the key pore-lining residues and revealed the bottleneck conformation of the carbapenem molecule during translocation. Additionally, we reverse mapped the CG structures of carbapenems to atomistic resolution in the bottleneck region to further illustrate the role of pore-lining residues in the translocation process. Finally, guided by the high-frequency contacts, we mutated two bulky pore-lining residues Y217A and F334A, to create OccD3m. The effect of mutations in OccD3m provided vital insight into the mechanism of carbapenem translocation.

2. CLASP WORKFLOW

Molecular understanding of the transport of drugs through biological barriers is fundamental to the future of biomedicine. There is a need to provide robust thermodynamic and kinetic data for the permeation of drugs that spans nano- to macro-scale. The key is to provide mechanistic, structural, orientational, conformational, and mutational details of the drug permeation process that can inform the development of new drugs and accelerate the sluggish drug discovery pipeline. To cover the spatial and temporal scales involved in the drug transport, we have adopted a multiscale approach that takes advantage of different resolutions. We use the state-of-the-art umbrella sampling method to compute the potential of mean force (PMF) of permeation of drugs through bacterial porins.

Umbrella sampling (US) simulations[45] are often laborious and typically require frequent user interventions at multiple steps. To streamline US simulations by eliminating the need for manual interventions, CLASP employs an efficient algorithm for the permeation of small molecules through bacterial porins. To maintain fast turnaround time in the current implementation of CLASP algorithm, we adopted coarse-grain (CG) resolution. Coarse-grain representation affords larger system sizes and longer timescale simulations by reducing the slow degree of freedom essential in all-atom simulations. Mapping the atomistic system to CG allows use of a time step that is one order of magnitude larger; plus, the CG resolution reduces the number of particles to be tracked in a simulation by at least one additional order of magnitude. Therefore, CG resolution is often two orders of magnitude more efficient than atomistic systems. The loss of atomic resolution in the CG simulations can be recovered by reverse mapping the output to atomistic representation.

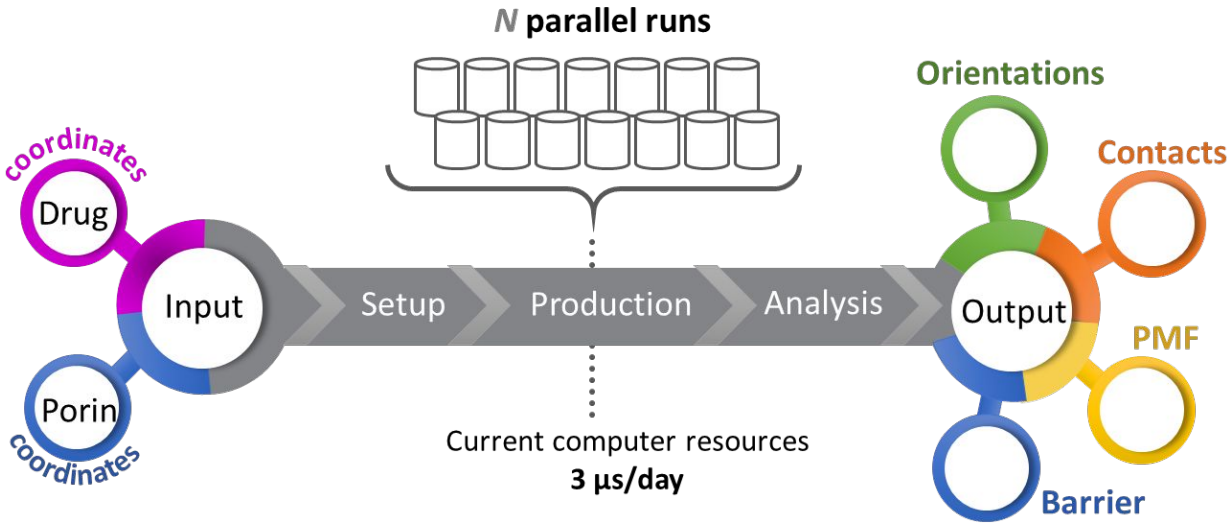

Figure 2. The CLASP workflow. The systematic representation of CLASP inputs and outputs. The porin and solute coordinates are the required inputs, which then are processed by the *C_setup.py* python script to generate N parallel umbrella sampling runs. The post simulation analysis scripts combine the N trajectories to generate the free energy profile, solute-protein residue contact map, and solute orientational analysis.

Among the several CG approaches available, MARTINI force field has been used for a diverse set of biomolecules, including lipids, proteins, solvents, and ions.[18,46-53] In our previous work, we developed MARTINI force field parameters for outer membrane lipids for several pathogenic and nonpathogenic Gram-negative bacterial species.[18,52-53] In CLASP, we retained the molecular descriptors of the proteins and substrate (here the carbapenems) at the level of MARTINI CG that recommends mapping four adjoining nonhydrogen atoms to one CG bead. This approach, popularly employed in biomolecular simulations, preserves the bonded and nonbonded interactions of the atomistic system and circumvents oversimplification of the molecular properties. The MARTINI CG has the advantage of transferability of the force field parameters to a wide range of biomolecules and on-demand reverse mapping to atomistic

resolution.[51] In addition, we employed the PyCGTOOL,[54] which semi-automates the parametrization process for obtaining CG models for small molecules.

The CLASP implementation is compatible with the GROMACS 5.0 simulation package.[55] The program uses a series of python scripts for building the input files, setting up parallel simulation runs, and performing post-simulation analysis. The workflow enables highly-automated simulations (Figure 2). The CLASP workflow and implementation used are described as follows.

CLASP input. The CLASP requires two inputs, the three-dimensional structure and coordinates of the bacterial outer membrane protein and the potential antibiotic or the solute molecule.

Solute molecule. The MARTINI force field parameters from the literature will be adopted for small molecules when available. Otherwise, we recommend employing the PyCGTOOL.[54] This python script generates the molecule's CG model parameters based on its atomistic dynamical data. The automated script provides molecular topologies and CG parameters with high chemical fidelity to the atomistic structure.

Bacterial outer membrane protein. The structure of the OccD3 bacterial protein is obtained from the Protein Data Bank. Missing residues are built via homology modeling using the standalone YASARA software[56] or online SWISS-MODEL server.[57] Next, the protein is embedded in a bacterial membrane and thermally equilibrated in the all-atom representation using standard MD packages or the CHARMM-GUI server.[58] The equilibrated protein is then converted to CG resolution using the MARTINI approach.

CLASP set up and production. In the setup stage, all systems are in the CG representation. The CG protein is embedded in CG bacterial lipids using Bacterial Outermembrane Builder script (*BOB.py*),[52-53] an in-house modified *insane.py* script[59] that includes CG parameters for bacterial outer membranes. The protein is embedded in an asymmetric patch of the outer membrane lipids and is solvated with standard MARTINI water. The system's energy is then minimized, followed by equilibration in the isothermal-

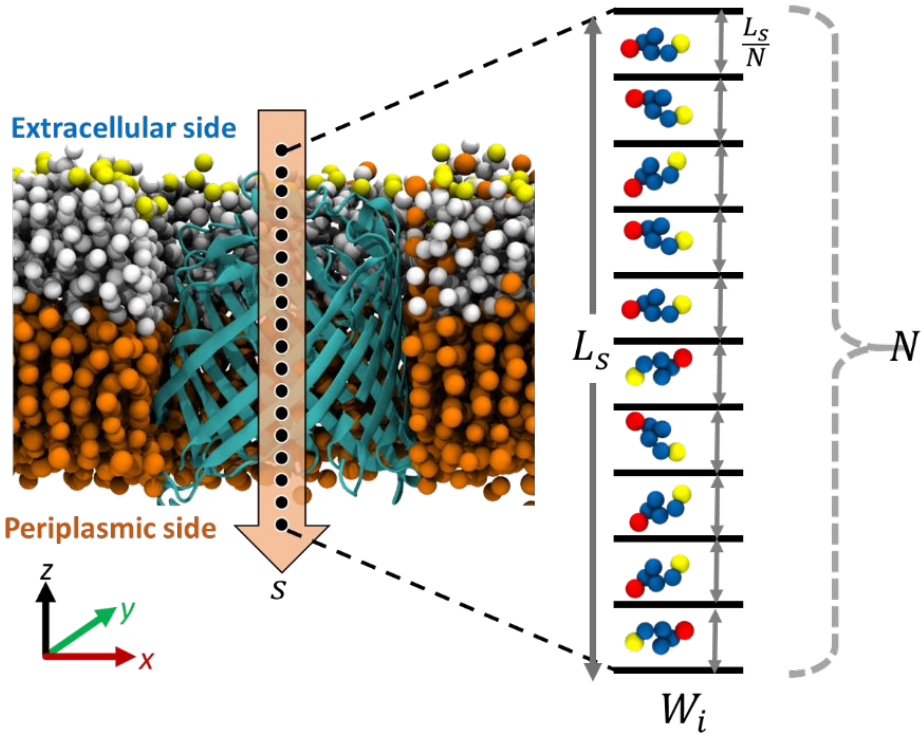

Figure 3. The CLASP simulation setup. The membrane embedded porin channel oriented parallel to the z-axis is divided into N equidistant umbrella sampling windows. The probe molecule is inserted into each W_i window.

isochoric (*NVT*) and isothermal-isobaric (*NPT*) conditions. The output of the *NPT* run is the starting structure for CLASP.

In the next step, bacterial membrane is generated in the *xy*-plane and the porin is embedded in the membrane such that the porin channel is along the *z*-axis. The molecule's permeation coordinate (s) is parallel to the z-axis, and the length of the porin channel from the extracellular region to the periplasmic region along s is denoted by L_s (Figure 3). The free energy profile along s is generated by dividing L_s into N umbrella sampling windows (W_i) with uniform spacing of L_s/N nm. The solute molecule is inserted in each W_i window, where the insertion coordinates are computed relative to the center-of-mass (COM) of the porin. Given, the hourglass shape of the porin, the COM lies in the middle of the porin channel. The location of the COM is considered $W_{N/2}$, with an equal number of windows on either side.

Next, the CLASP script generates N separate folders, each with a unique location of the substrate molecule defined within W_i, totaling the length L_s along s. Each folder is set up to execute energy minimization and US simulations independently. The N jobs run concurrently on separate computer cluster nodes for maximum efficiency and shortest completion time.

CLASP analysis. The CLASP outputs are four primary outputs from a CLASP run:

Free energy profile. The potential of mean force (PMF) profile of the solute molecule's transport from the extracellular to the periplasmic region is computed along the one-dimensional translocation coordinate (s) .The *C_PMF.py* script combines the trajectories from the N folders to generate the PMF profile of the solute molecule. The PMF average profile with standard deviations were obtained using a GROMACS built-in utility. The detailed usage of the script is provided in the Supporting Information.

Permeation barrier. the barrier height (*BH*) for the solute's permeation is calculated by taking the difference between the maximum and the minimum energy points along s. Using the transition state theory as a first-order approximation of the solute translocation, we defined rate constant as $k = (k_B T/h) exp^{(-BH/RT)}$, where k_B is the Boltzmann constant, *R* is the gas constant, and *T* is the temperature.

Orientational analysis. The orientation of the solute molecule is quantified by defining the interatomic vector connecting head bead to the tail bead of the solute molecule, $\vec{r} = \overrightarrow{r_T} - \overrightarrow{r_H}$. Based on the angle θ that the unit vector $\hat{d} = \frac{\vec{r}}{|r|}$ makes with the z-axis, we used $d_z = |d| \cos\theta$ to determine in the orientation of the molecule, where $d_z \in [-1, 1]$. If $d_z = 1$, the molecule is orientated headfirst towards the translocation direction, and $d_z = -1$ for tail first. If $d_z = 0$, then the molecule lies in the *xy*-plane, perpendicular to the *z*-axis.

Contact analysis. The interaction of the solute molecule with the protein residues is performed for all N windows. A contact is defined to have formed between the solute and protein residue if the distance between any of their beads is within a 1.2 nm cut off. A contact receives a value of either 1 when formed or 0 when the contact is broken. The cumulative number of contacts made by the solute with each protein residue in N windows is calculated. The residues are sorted from smallest to largest based on the total number of residue-solute contacts to identify the highest contacting residues (99th percentile).

Reverse mapping. The on-demand CG to atomistic reverse mapping is available to determine the atomistic level interactions of the solute molecule with the pore-lining residues.[51]

3. METHODS

Carbapenem coarse graining. The MARTINI CG parameters for the carbapenem molecules were developed based on many-to-one mapping. PyCGTOOL was used to generate the CG coordinates and topologies for all solute molecules. Benchmarking of the CG parameters against the atomistic models was performed using the PyCGTOOL. The CG mapping of the carbapenem molecules are shown in Figure 4. The force field parameters of all six carbapenems are provided in Tables S1-S6.

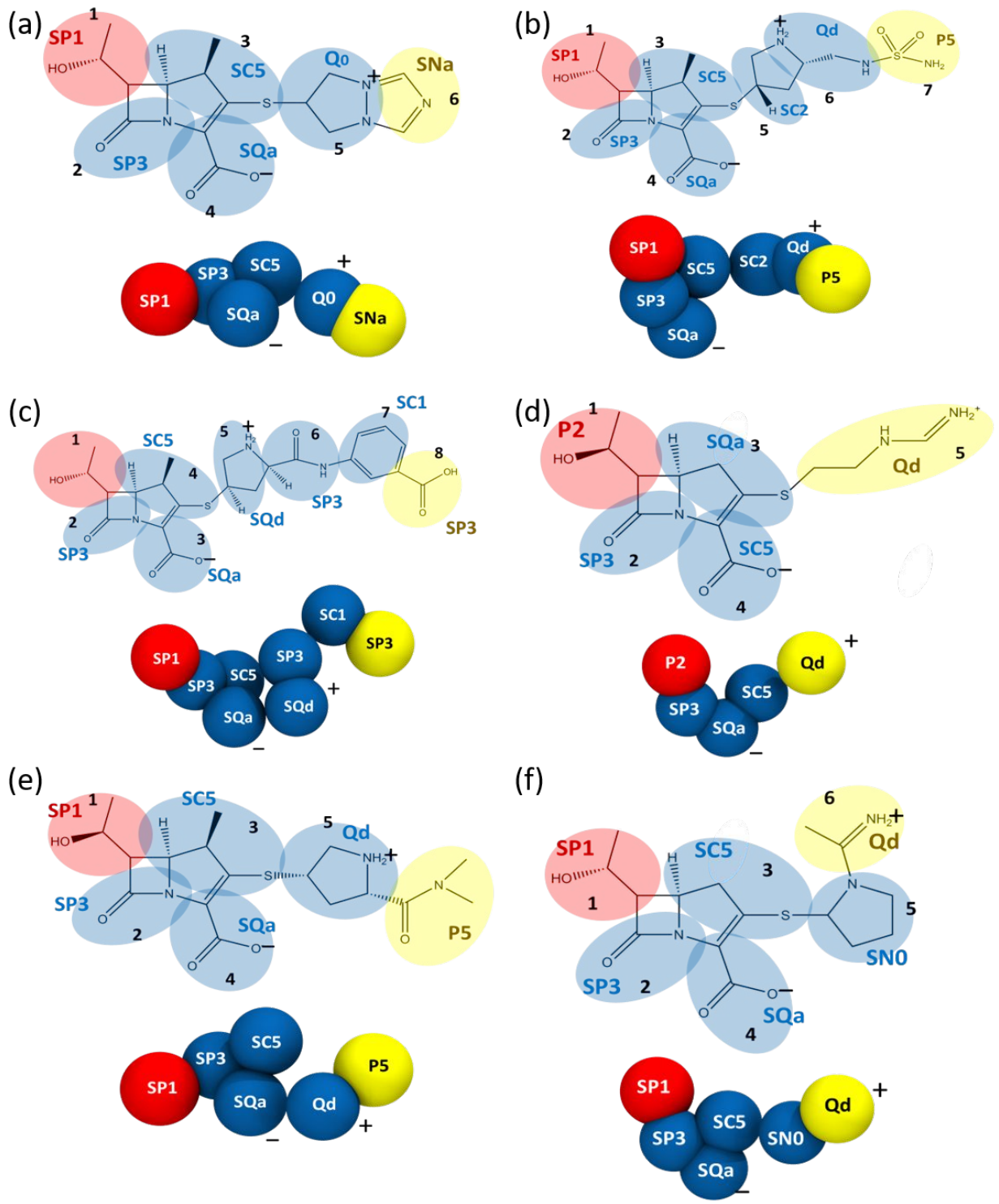

Figure 4. Atomistic to CG mapping for (a) biapenem, (b) doripenem, (c) ertapenem, (d) imipenem, (e) meropenem, and (f) panipenem showing the MARTINI bead type assignments along with positive and negative charges. The red bead, which is part of the β-lactam ring, denotes the head and the yellow bead, the farthest bead from the β-lactam ring, denotes the tail.

Porin structure. The x-ray crystallographic structure of OccD3 was obtained from the Protein Data Bank (PDB ID: 3syb), and the missing residues were built using the SWISS-MODEL server. The structure was

then optimized in atomistic representation using the CHARMM36 force field.[60] The *NVT* and *NPT* simulations were performed for 200 ns each at T = 320 K. The point mutations in the OccD3 structure were generated using the CHARMM-GUI webserver.[58] The mutated structures were then optimized using the same approach outlined above for the OccD3.

Porin-membrane system. The CG mapping of the OccD3 was performed using *martinize.py* script. The MARTINIv2.1 force field parameters[49] were used along with the ELNeDyn network[48] constraint to maintain the porin's secondary structure. The porin was inserted in a 10×10 nm^2 patch of the *P. aeruginosa* membrane using the *BOB.py* script. The membrane's outer leaflet consisted of *P. aeruginosa*'s lipid A and 1,2-dipalmitoyl-sn-glycero-3-phosphoethanolamine (DPPE) in 9:1 ratio and pure DPPE in the lower leaflet. The membrane was placed in a 10×10×12 nm^3 simulation box and solvated with MARTINI water (9:1 of W:WF) and 150 mM $CaCl_2$. The molecular composition of the simulation box is provided in Table S7.

CG MD Simulation. The GROMACS 5.1.2 package[55] was used for CG MD simulations. The system was energy minimized using the steepest-decent algorithm until the maximum force on any bead was below the tolerance parameter of 10 $kJmol^{-1}nm^{-1}$. This was followed by *NVT* and *NPT* equilibration for 0.02 μs and 2 μs, respectively. A 20 fs time step was used for the equilibration and production runs. The temperature was set to 320 K for all systems using the v-rescale thermostat with τ_t = 1 ps. A semi-isotropic pressure coupling of 1 bar was maintained using Berendsen barostat[61] with τ_p = 4 ps. Both the nonbonded van der Waals and electrostatics interaction cut offs were set to 1.2 nm. Periodic boundary conditions were applied in all three dimensions.

CLASP production. A total of N independent simulations were perfomed concurrently on separate computer nodes (Table S8). Within each window the simulations were performed in two steps. The first US run was performed for 0.2 μs using a 20 fs time step. The OccD3 protein and the solute molecule were position-restrained with a 1000 $kJmol^{-1}nm^{-2}$ force constant. In the second step, the US simulation was run for 1 μs with a 20 fs time step. The position restraint of the drug molecule was removed in this step with all other parameters maintained. The harmonic potential with a force constant of 3000 $kJmol^{-1}nm^{-2}$ was used. A cut off of 1.1 nm was used for both the long-range electrostatic and the nonbonded van der Waals interactions. The potential-shift-Verlet algorithm was applied to shift the van der Waals interactions beyond the cut off. The Coulombic interactions were calculated using the reaction-field algorithm. The temperature was maintained at 300 K using the v-rescale thermostat with τ_t = 1.0 ps.

Analysis. Post simulation analyses were performed using CLASP python scripts. We computed the histograms of the US window along the translocation path (Figures S1-S6). The CAVER plugin[62] available in PyMOL was used for OccD3 channel analysis. Molecular visualization and graphics were generated using VMD,[63] PyMOL,[64] and YASARA.[56]

4. RESULTS AND DISCUSSION

The CLASP simulations were employed to characterize and compare the permeabilities of six carbapenems— biapenem, doripenem, ertapenem, imipenem, meropenem, and panipenem—through the wildtype OccD3 porin. The role of pore-lining residues involved in carbapenem translocation was further evaluated by site-directed mutagenesis of Y217 and F334 residues to alanine in the double mutant OccD3 (OccD3m) porin. The results provided detailed insight into the uptake mechanism and demonstrated the robustness of the CLASP method in capturing the effects of point mutations.

4.1 Carbapenem uptake through OccD3 channel with characteristic PMF

The PMF profile of each carbapenem molecule's transport from the extracellular to the periplasmic region of the OccD3 porin was studied in the $s \in [0, 11]$ nm range. For clarity, in this discussion, the s coordinate is subdivided into three sections—the extracellular region with the porin vestibule, $s \in [0 - 4.2]$ nm; the porin constriction region, $s \in [4.2 - 7.4]$ nm; and the periplasmic region, $s \in [7.4 - 11.0]$ nm.

In the extracellular region, the carbapenem molecule interacts freely with the porin loops and shows an energy minimum at the pore vestibule $s = 4.2$ nm. Each carbapenem is different in molecular size (Table 1) and functional groups attached to the β-lactam ring (Tables S1-S6), so free energy variations among the carbapenems are expected; however, stabilization before penetrating the porin channel is observed in all six cases (Figure 5). The free energy profile of all six carbapenems except doripenem show approximately 10 kcal mol^{-1} stabilization at $s = 4.5$ nm. Beyond the extracellular vestibule, the free energy increases for all carbapenems until they reach the bottleneck.

Table 1. Molecular weight (MW), barrier height (*BH*), and rate constant (*k*) of six carbapenems through OccD3 and OccD3m.

Antibiotic	MW (Da)	OccD3		OccD3m	
		BH (kcal mol^{-1})	*k* (s^{-1})	*BH* (kcal mol^{-1})	*k* (s^{-1})
Biapenem	350.4	27±2.5	1.4×10^{-7}	15±2.1	7.6×10^{1}
Doripenem	420.5	20±3.2	1.7×10^{-2}	16±2.2	1.4×10^{1}
Ertapenem	474.5	31±2.8	6.0×10^{-12}	10±2.5	2.1×10^{-5}
Imipenem	299.4	22±2.1	1.1×10^{-4}	16±1.6	1.4×10^{1}
Meropenem	383.5	21±1.8	3.3×10^{-3}	14±1.6	4.1×10^{2}
Panipenem	339.4	26±2.3	7.5×10^{-7}	12±2.2	1.2×10^{4}

A comparison of the free energy barrier for translocation through the OccD3 pore shows a range between 20-31 kcal mol^{-1} (Table 1). In OccD1, the translocation barriers for positively charged amino acid substrates vary between 5-10 kcal mol^{-1}.[20] Energy barriers are three to four times higher for permeation through OccD3 than OccD1, which is expected because OccD3 has more constrained channel and contains a unique N-terminal extension loop.[34]

We observe a weak correlation between the magnitude of the energy barrier and the molecular size of the carbapenem molecule. Ertapenem is the largest carbapenem and has the highest *BH* = 31±2.8 kcal mol^{-1}. Imipenem, which is the smallest carbapenem, has one of the smallest *BH* = 22±2.1 kcal mol^{-1}. The similarly sized, biapenem and panipenem, have energy barriers of *BH* = 27±2.5 and 26±2.3 kcal mol^{-1}, respectively. Meanwhile, doripenem, which is the second largest in terms of MW, has the lowest *BH* = 20±3.2 kcal mol^{-1}. The results indicate that the molecular size of the carbapenems is not the only criteria that determines the magnitude of the energy barrier. In a previous study, Soundararajan *et al*., reported that meropenem interacts more strongly with the OccD3 porin than imipenem using ion conductance measurements[34]; however Table 1 shows that both molecules have similar barrier heights. To investigate the differences in energy barriers, we evaluated the interactions of carbapenem molecule throughout the porin channel with emphasis on the bottleneck region. A detailed discussion of the carbapenem conformation at the bottleneck region of the pore is provided in Section 4.3.

The rate constant (s^{-1}) of the six carbapenems are shown in Table 1. Rate constants are calculated by assuming a first order transition state theory and are directly related to energy barriers. They are used to distinguish the relative rate and preference of carbapenems permeating through OccD3. Between ertapenem (*BH* = 31±2.8 kcal mol^{-1}) and doripenem (*BH* = 20±3.2 kcal mol^{-1}), which has the largest and smallest energy barriers, the rate constants are different by multiple orders of magnitudes. We further compare the rate constants of mutations, which will be discussed in Section 4.4

It is apparent from the thermodynamic that besides the molecular size of the translocating molecule, the orientation of the molecule in pore's constriction region can also be crucial. For this purpose, we evaluated the orientation of the carbapenem molecule along $s \in [0 - 11.0]$ nm. The orientation profiles of the six carbapenems were somewhat similar in the extracellular and periplasmic regions. In all cases, the carbapenem adopted a wide range of orientations, indicated by the large deviation in the average d_z values in both the extracellular region $s \in [0 - 4.2]$ nm and the periplasmic region, $s \in [7.4 - 11.0]$ nm (Figure 6).

However, in the constriction zone, the solute molecule is restrained by the channel walls, which was manifest in small deviations in the d_z values.

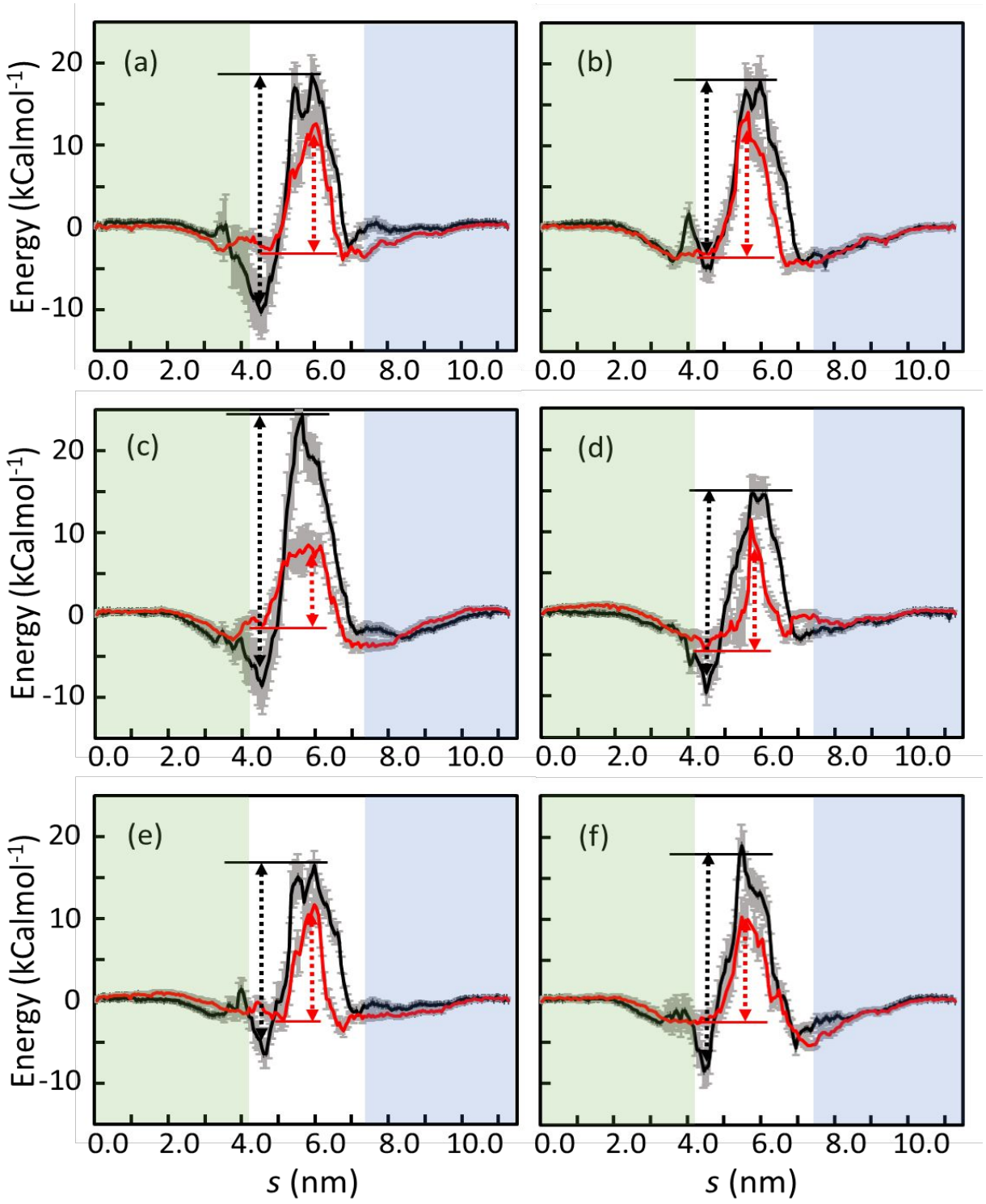

Figure 5. The PMF profiles of carbapenems through OccD3 and OccD3m. The comparison of (a) biapenem, (b) doripenem, (c) ertapenem, (d) imipenem, (e) meropenem, and (f) panipenem translocation through OccD3 (black line) and OccD3m (red line). The error bars calculated using the bootstrap analysis are marked in gray. The barrier heights (dashed lines) are marked in each panel. The translocation coordinate (*s)* is subdivided into outer membrane region (green), constriction zone (white) and periplasmic region (blue).

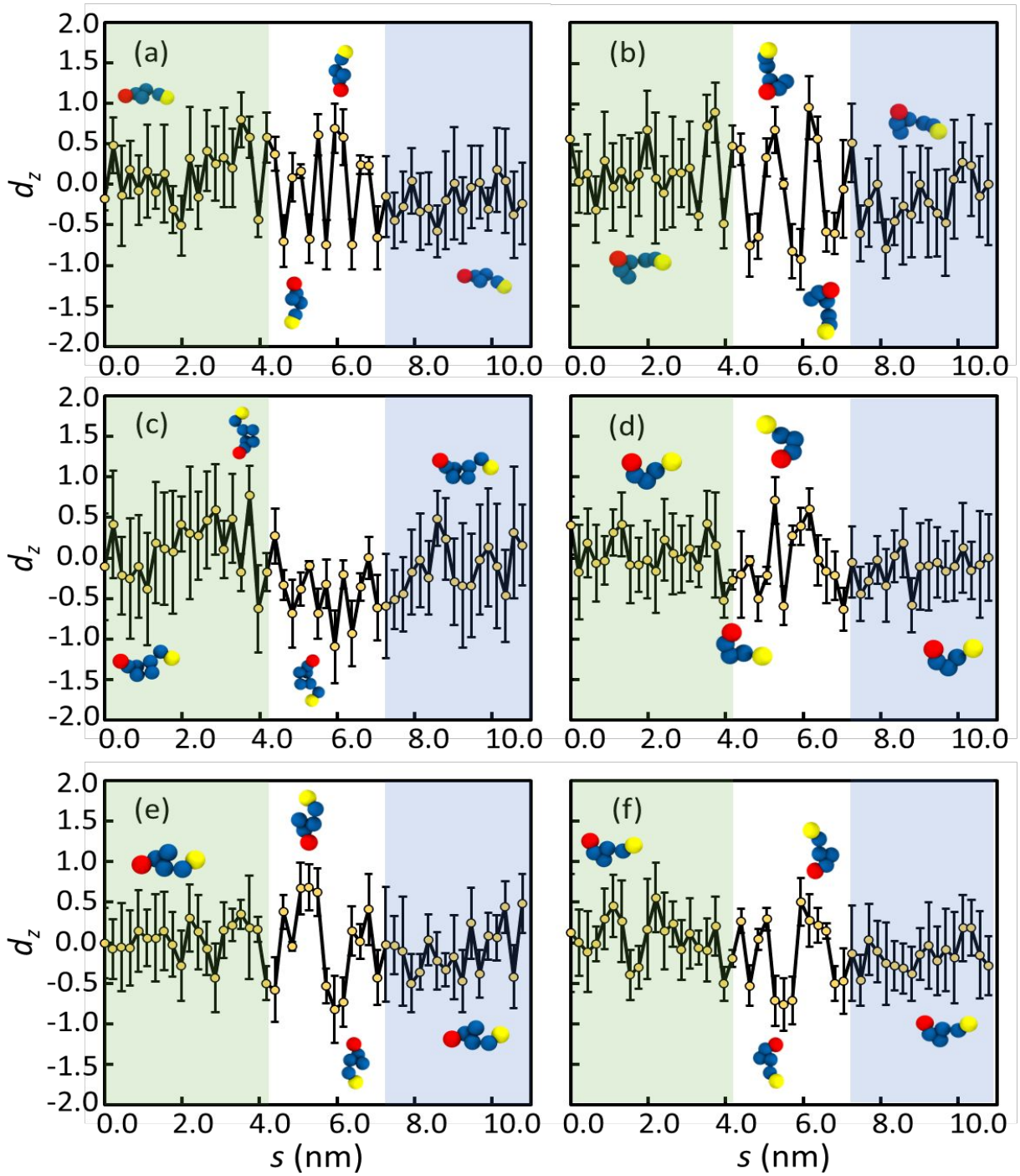

Figure 6. Orientational analysis of carbapenems along the translocation coordinate in OccD3. The variation in d_z for (a) biapenem, (b) doripenem, (c) ertapenem, (d) imipenem, (e) meropenem, and (f) panipenem as a function of s. The mean d_z values are denoted by the yellow dots, and the standard deviations are shown by the black bars. The s coordinate is subdivided into outer membrane region (green), constriction region (white) and periplasmic region (blue).

4.2 Carbapenems make highest contact with bulky Y217 and F334 OccD3 residues

Using the molecular interaction data of the carbapenem molecules with the OccD3 residues, we generated the contact maps. The contact map provides a percentile-based overview of contacts the molecule makes with each of the 452 OccD3 residues (Figure 7). All carbapenems have the same set of highest contact residues, namely Y169, Y217, Y326, H328, and F334 (Figures S7-S12). In fact, comparing the full contact map between all carbapenems, the most contacted residues (>80th percentile) are consistent. This reflects the dominant role of these residues in kinetics of carbapenem uptake. Besides, the importance of the charged D342 and R449 residues was shown by Soundarajan *et al.* in the ion-conductance experiments involving molecular uptake of imipenem and meropenem via OccD3 porin; the authors demonstrated that both mutations D342H (charge reversal) and R449A (charge neutralization) disturbed the translocation of imipenem and meropenem molecules.[34]

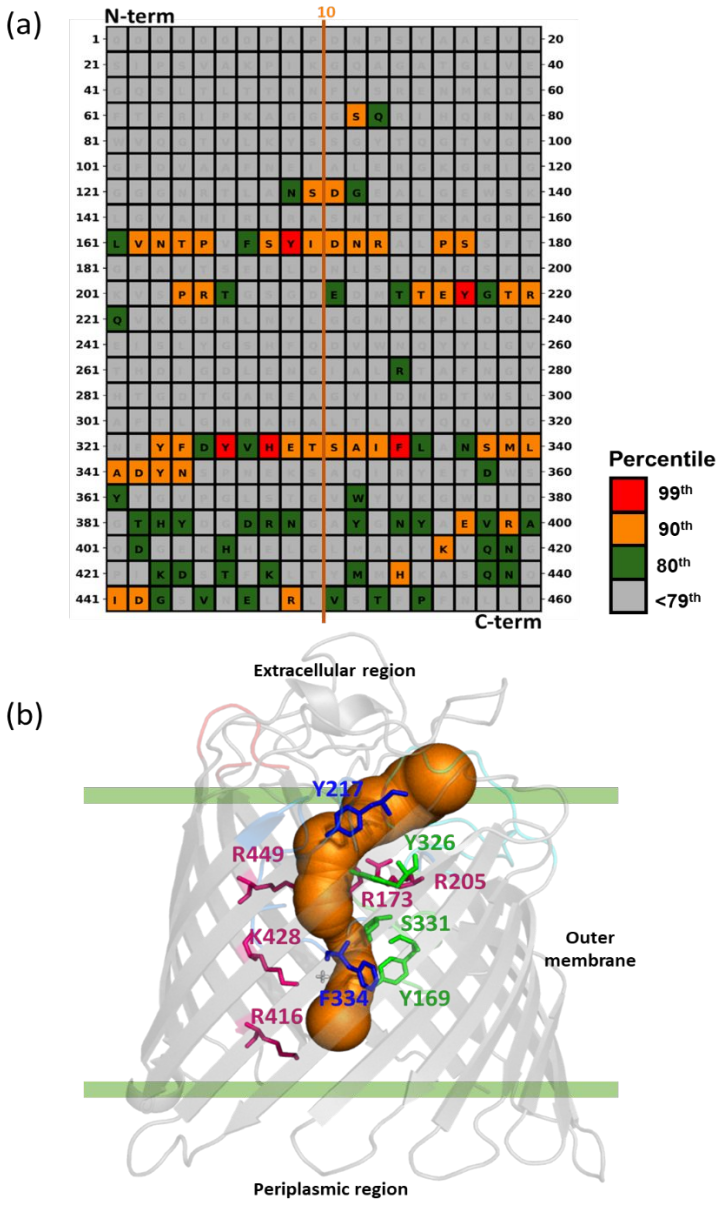

Figure 7. Interaction of meropenem with OccD3 porin channel. (a) Meropenem-OccD3 contact map, and (b) structure of the OccD3 (cartoon representation, gray) along with key pore-lining residues (stick model) that line the channel (orange, surface representation).

Notably, in OccD1 carbapenem transporter, residues Y176, Y282, D307, Y305 and D295 have been reported as the most probable pore-lining residues;[20] the sequence alignment between OccD3 and OccD1 (Table S9) shows that Y176 and Y282 in OccD1 match Y217 and Y326 (99th percentile residues) in OccD3, and D307, Y305 and D295 in OccD1 match D342, L340 and S331 (90th percentile residues) in OccD3. These results confirm that both OccD3 and OccD1 are carbapenem transporters.

All six carbapenems make contacts with a series of charged arginine and lysine residues (Figures S7-S12), which constitutes the basic ladder. These observed interactions with the charged residues are consistent with the earlier reports involving uptake of substrates via OccD3 and OccD1 porins. The presence of the basic ladder is considered crucial in providing the Coulombic interactions for the substrate to translocate through the porin channel.

Previous experimental and computational studies have focused on evaluating the role of charged residues in OccD3 and OccD1 channels.[34,39] However, the steric effect of bulky pore-lining residues in OccD3 channel have not been investigated. Using CLASP, we explore the effect of two bulky residues—F334 and Y217—that make the first and second highest frequency contacts in all six carbapenems. As shown in Figure 7b, Y217 lies at the tip of the constriction zone on the extracellular side. The F334 is the most important hydrophobic residue

in OccD3 that contacts all six carbapenems in their highest energy structures. We hypothesized that a double mutation of bulky residues Y217 and F334 to alanine would increase channel diameter and lower the energy barrier to carbapenem permeation. We also expect that these mutations will not cause the carbapenem to adopt a new pathway in the channel.

Remarkably, in OccD3m, the top residue contacts (99th percentile) for all six carbapenems are identical as well (Y169, N172, R173, Y326, S331), and the top 90th percentile contacts are fairly consistent (Figure S7-S12). Contact maps of OccD3 and OccD3m have similar most-contacted residues regions, which confirms the presence of a single pathway through the porin. The double mutation shows that the two bulky residues play a significant role in creating the bottleneck in the porin pathway. The discussion on the mechanism of carbapenem translocation through OccD3m is provided in Section 4.4.

4.3 Conformation of the carbapenem at the bottleneck in the OccD3 channel influence the energy barrier to translocation

The orientational and contact map analysis of the carbapenem molecules in the OccD3 channel indicates the strong interplay between the carbapenem structure and the pore-lining residues in determining the energy barrier to the translocation. The chemical groups attached to the β-lactam ring in different carbapenems impact the conformational flexibility of the molecule, which can be an important factor at the pore's bottleneck region.

For this purpose, we reverse mapped the carbapenem molecule and porin from CG to atomistic resolution and evaluated their molecular interactions in the bottleneck conformation. In biapenem, the molecule is oriented tail first with $d_z = -1.0$ at $s = 5.4$ nm, and then fliped to $d_z = 0.9$ after the bottleneck (Figure S13). At $s = 5.4$ nm, biapenem showed interactions with Y169, N172, F334, and M339. These interactions were also observed as high frequency contacts (90th percentile) in the contact map (Figure S7).

Doripenem was in a folded-state with the β-lactam ring pointing towards the periplasm at $s = 6.1$ nm, which corresponds to the bottleneck region (Figure S14). The contacting pore residues are N163, P165, Y169, and F334; the former three residues can be found from the high (90th percentile) contacts and F334 belongs to the group of the highest (99th percentile) frequency contacts (Figure S8).

The ertapenem molecule is fully extended and is aligned with its tail pointing towards the periplasm (Figure S15). This orientation is maintained for much of the constriction zone for s from 4.5 to 6.5 nm beyond which the molecule eases out of the fixed orientation as it diffuses out to the periplasmic region. As expected, ertapenem is the largest carbpenem we studied (MW 474.5 Da), and it does experience the highest energy barrier to the translocation. At $s = 5.7$ nm, the molecule makes multiple contacts with pore-lining residues. These residues include the bulky Y169 and F334 that constrict the channel, and polar residues N172, S331, and S338 that provide stabilization.

Imipenem is the smallest of the six carbapenems and is able to translocate through the pore in an oblique orientation with $d_z = -0.5$ (Figure S16). The primary residue contacts at the highest point in energy profile are I170, S331, and F334, which unlike the other five carbapenems, does not include Y169. As a result of the small size of imipenem, fewer bulky contacts are experienced and therefore, reducing the energy barrier to translocation.

Meropenem has an orientational profile similar to imipenem. The contacting residues at $s = 5.6$ nm include the bulky Y169 and F334 residues, nonpolar I170, polar S168, and charged D171 (Figure S17). The orientation of the molecule causes it be in contact with residues that have high variability in their side chain size and polarity. Despite the slightly bigger size of meropenem from the six carbapenems, it has a quite small energy barrier.

Panipenem is a relatively small carbapenem (MW 339 Da) and it underwent only a few orientational flips as it navigated the constriction zone. At the highest energy point, the molecule adopted an L-shaped

geometry with $d_z = 1.0$ (Figure S18). The contacting residues include four bulky groups Y169, Y217, Y326, F334, and polar D171.

This work demonstrates that the differences in the carbapenem orientation, contacting residues, and location of the bottleneck along the translocation path are the contributing factors to the varibality in the energy barrier and the translocation rates. This detailed analysis is possible due to the robustness of the CLASP alogirthm that can provide the on-demand reverse mapped structure of the simualtion system at atomistic-level precision.

4.4 Carbapenems have lower permeation barrier through OccD3m

The free energy profile of each carbapenem through OccD3m (Figure 5, red lines) show lower barriers than through OccD3. The barrier heights and rate constants results of carbapenems via OccD3m and OccD3 channels are provided in Table 1.

Interestingly, the largest change in barrier height for translocation occurred in ertapenem (ΔBH = 21 kcal mol^{-1}), the largest carbapenem in the group studied. In contrast, one of the smallest changes in all six carbapenems occurred with imipenem (ΔBH = 6 kcal mol^{-1}), the smallest carbapenem in the group. A close up view of ertapenem's molecular interactions with OccD3 and OccD3m at $s = 5.8$ nm, the highest energy point, reveals the reason for the change in free energy (Figure 8). The minimum in OccD3m is possible because the large ertapenem molecule is stabilized by the added volume created by concurrent Y217A and F334A mutations; none of the other five carbapenems were large enough to experience this dual volume increase.

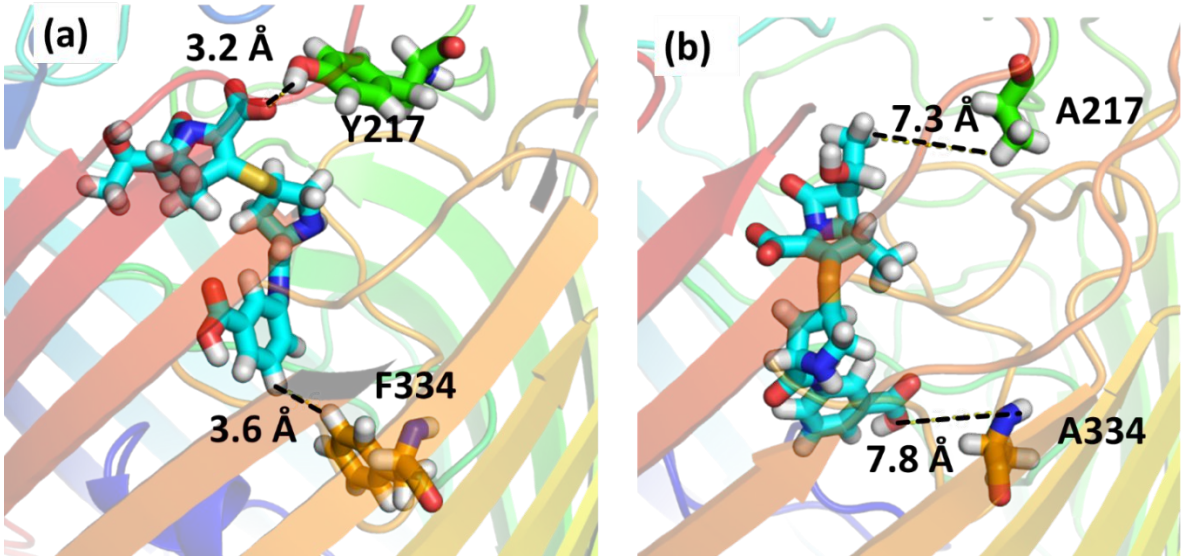

Figure 8. Comparison of reserve-mapped atomistic structure and orientation of ertapenem in the bottleneck region, $s = 5.8$ nm of (a) OccD3 and (b) OccD3m channel. The contacts the molecules make with the pore-lining residues in their highest energy conformation. The porin is shown in ribbon representation (blue to red from N-term to C-term) and ertapenem is shown as sticks (C cyan; O red; H white; S gold; and N blue). The pore-lining residues are shown in stick representation Y217 and A217 (C green), and F334 and A334 (C orange); the other atoms have same color scheme as in ertapenem.

Furthermore, the orientational profile comparison of the six carbapenems through OccD3 and OccD3m supports our hypothesis that Y217 and F334 influence the translocation behavior. The carbapenem orientational analysis for translocation through the OccD3m pore shows a higher number of flips in the constriction region (Figure S19). The widening of the pore provides small pockets for the molecules to orient in different conformations as they navigate the translocation coordinate.

5. CONCLUSIONS

Here we report the developement of a new computational screening platform called CLASP that is designed to accelerate the antibiotic discovery process. This computational platform provides an automated screening of small molecules by quantifying their permeabilities through the bacterial outer membrane porins. The CLASP outputs comprehensive thermodynamic data, which includes, potential of mean force profile, energy barrier, translocation rate constant, contact analysis of the molecule with the pore-lining residues, orientation analysis of the molecule within the porin, and the overall mechanism of the antibiotic uptake. Additionally, the fast turnaround times will enable the establishment of structure-property relationships among molecular species that have high bacterial membrane permeability.

In this first application of CLASP, we demonstrate the permeability profile of six, well-established antibiotics from the carbapenem family through *P. aeruginosa*'s OccD3 channel. The proof-of-concept study was undertaken to use the known literature and illustrate the permeability profiles for biapenem, doripenem, ertapenem, imipenem, meropenem, and panipenem. The results show excellent agreement with the barrier heights, the key residues, and the translocation rate constants of the drug molecules. We were able to identify critical pore-lining residues in the OccD3 channel that provide steric gating. Mutation of these residues to less bulky groups enhanced the predicted rates. Moreover, the wall-clock time to simulate one antibiotic molecule was less than two hours based on the current computational resource.

In conclusion, our goal was to advance strategies that will facilitate the identification of new antibiotics. This work has enabled comprehensive characterization of antibiotic uptake through bacterial envelope. In the future, we plan to employ CLASP to screen large natural compound libraries to identify the new potential antibiotics.

ACKNOWLEDGMENTS

This work is supported by the National Science Foundation grant numbers CBET-1706061 and DMR-1757749. Computational resources were provided by Information and Technology Services at Syracuse University (Eric Sedore, Larne Pekowsky, and Michael R. Brady) as well as the Extreme Science and Engineering Discovery Environment (XSEDE), which is supported by National Science Foundation grant number ACI-1053575. The authors thank Somya Chakraborty for the help with the manuscript.

SUPPORTING INFORMATION

The contents include: description of the CLASP python scripts, coarse grain-mapping of the six antibiotics, simulation setup details, contact maps, and reversed mapped orientational analysis of the antibiotics in OccD3 channel, and orientational analysis of carbapenems along the translocation coordinate in OccD3m.

References

1. Davies, J.; Davies, D., Origins and evolution of antibiotic resistance. *Microbiology and Molecular Biology Reviews* **2010,** *74*, 417.
2. Blair, J. M. A.; Webber, M. A.; Baylay, A. J.; Ogbolu, D. O.; Piddock, L. J. V., Molecular mechanisms of antibiotic resistance. *Nature Reviews Microbiology* **2015,** *13*, 42-51.
3. Frieri, M.; Kumar, K.; Boutin, A., Antibiotic resistance. *Journal of Infection and Public Health* **2017,** *10*, 369-378.
4. Martens, E.; Demain, A. L., The antibiotic resistance crisis, with a focus on the united states. *Journal of Antibiotics* **2017,** *70*, 520-526.
5. Levy, S. B.; Marshall, B., Antibacterial resistance worldwide: Causes, challenges and responses. *Nature Medicine* **2004,** *10*, S122-S129.
6. Luepke, K. H.; Suda, K. J.; Boucher, H.; Russo, R. L.; Bonney, M. W.; Hunt, T. D.; Mohr, J. F., Past, present, and future of antibacterial economics: Increasing bacterial resistance, limited antibiotic pipeline, and societal implications. *Pharmacotherapy* **2017,** *37*, 71-84.
7. Andersson, D. I.; Hughes, D., Antibiotic resistance and its cost: Is it possible to reverse resistance? *Nature Reviews Microbiology* **2010,** *8*, 260-271.
8. Brooks, B. D.; Brooks, A. E., Therapeutic strategies to combat antibiotic resistance. *Advanced Drug Delivery Reviews* **2014,** *78*, 14-27.
9. Rossiter, S. E.; Fletcher, M. H.; Wuest, W. M., Natural products as platforms to overcome antibiotic resistance. *Chemical Reviews* **2017,** *117*, 12415-12474.
10. Tacconelli, E.; Carrara, E.; Savoldi, A.; Harbarth, S.; Mendelson, M.; Monnet, D. L.; Pulcini, C.; Kahlmeter, G.; Kluytmans, J.; Carmeli, Y.; Ouellette, M.; Outterson, K.; Patel, J.; Cavaleri, M.; Cox, E. M.; Houchens, C. R.; Grayson, M. L.; Hansen, P.; Singh, N.; Theuretzbacher, U.; Magrini, N.; Workin, W. H. O. P. P. L., Discovery, research, and development of new antibiotics: The who priority list of antibiotic-resistant bacteria and tuberculosis. *Lancet Infectious Diseases* **2018,** *18*, 318-327.
11. Delcour, A. H., Outer membrane permeability and antibiotic resistance. *Biochimica Et Biophysica Acta-Proteins and Proteomics* **2009,** *1794*, 808-816.
12. Nikaido, H., Molecular basis of bacterial outer membrane permeability revisited. *Microbiology and Molecular Biology Reviews* **2003,** *67*, 593-+.
13. Vergalli, J.; Bodrenko, I. V.; Masi, M.; Moynié, L.; Acosta-Gutiérrez, S.; Naismith, J. H.; Davin-Regli, A.; Ceccarelli, M.; van den Berg, B.; Winterhalter, M.; Pagès, J.-M., Porins and small-molecule translocation across the outer membrane of gram-negative bacteria. *Nature Reviews Microbiology* **2020,** *18*, 164-176.
14. Liu, J.; Wolfe, A. J.; Eren, E.; Vijayaraghavan, J.; Indic, M.; van den Berg, B.; Movileanu, L., Cation selectivity is a conserved feature in the occd subfamily of pseudomonas aeruginosa. *Biochim Biophys Acta* **2012,** *1818*, 2908-2916.
15. Dam, S.; Pages, J. M.; Masi, M., Stress responses, outer membrane permeability control and antimicrobial resistance in enterobacteriaceae. *Microbiology (Reading, England)* **2018,** *164*, 260-267.
16. Nikaido, H., Porins and specific channels of bacterial outer membranes. *Molecular Microbiology* **1992,** *6*, 435-442.
17. Pages, J. M.; James, C. E.; Winterhalter, M., The porin and the permeating antibiotic: A selective diffusion barrier in gram-negative bacteria. *Nature Reviews Microbiology* **2008,** *6*, 893-903.
18. Ma, H. L.; Khan, A.; Nangia, S., Dynamics of ompf trimer formation in the bacterial outer membrane of escherichia coli. *Langmuir* **2018,** *34*, 5623-5634.
19. Parkin, J.; Khalid, S., Atomistic molecular-dynamics simulations enable prediction of the arginine permeation pathway through occd1/oprd from pseudomonas aeruginosa. *Biophysical Journal* **2014,** *107*, 1853-1861.
20. Samanta, S.; Scorciapino, M. A.; Ceccarelli, M., Molecular basis of substrate translocation through the outer membrane channel oprd of pseudomonas aeruginosa. *Physical Chemistry Chemical Physics* **2015,** *17*, 23867-23876.
21. Samsudin, F.; Khalid, S., Movement of arginine through oprd: The energetics of permeation and the role of lipopolysaccharide in directing arginine to the protein. *Journal of Physical Chemistry B* **2019,** *123*, 2824-2832.

22. Somboon, K.; Niramitranon, J.; Pongprayoon, P., Probing the binding affinities of imipenem and ertapenem for outer membrane carboxylate channel d1 (occd1) from p. Aeruginosa: Simulation studies. *Journal of Molecular Modeling* **2017,** *23*.
23. Eren, E.; Parkin, J.; Adelanwa, A.; Cheneke, B.; Movileanu, L.; Khalid, S.; van den Berg, B., Toward understanding the outer membrane uptake of small molecules by pseudomonas aeruginosa. *The Journal of biological chemistry* **2013,** *288*, 12042-53.
24. Pothula, K. R.; Solano, C. J. F.; Kleinekathöfer, U., Simulations of outer membrane channels and their permeability. *Biochimica et Biophysica Acta (BBA) - Biomembranes* **2016,** *1858*, 1760-1771.
25. Bajaj, H.; Scorciapino, M. A.; Moynie, L.; Page, M. G.; Naismith, J. H.; Ceccarelli, M.; Winterhalter, M., Molecular basis of filtering carbapenems by porins from beta-lactam-resistant clinical strains of escherichia coli. *The Journal of biological chemistry* **2016,** *291*, 2837-47.
26. D'Agostino, T.; Salis, S.; Ceccarelli, M., A kinetic model for molecular diffusion through pores. *Biochimica et Biophysica Acta (BBA) - Biomembranes* **2016,** *1858*, 1772-1777.
27. Subramanian, N.; Condic-Jurkic, K.; Mark, A. E.; O'Mara, M. L., Identification of possible binding sites for morphine and nicardipine on the multidrug transporter p-glycoprotein using umbrella sampling techniques. *J Chem Inf Model* **2015,** *55*, 1202-17.
28. Padhi, S.; Priyakumar, U. D., Urea–aromatic stacking and concerted urea transport: Conserved mechanisms in urea transporters revealed by molecular dynamics. *Journal of Chemical Theory and Computation* **2016,** *12*, 5190-5200.
29. Hamelberg, D.; Mongan, J.; McCammon, J. A., Accelerated molecular dynamics: A promising and efficient simulation method for biomolecules. *The Journal of chemical physics* **2004,** *120*, 11919-29.
30. Hancock, R. E. W.; Brinkman, F. S. L., Function of pseudomonas porins in uptake and efflux. *Annual Review of Microbiology* **2002,** *56*, 17-38.
31. Strateva, T.; Yordanov, D., Pseudomonas aeruginosa - a phenomenon of bacterial resistance. *Journal of Medical Microbiology* **2009,** *58*, 1133-1148.
32. *Antibiotic resistance threats in the united states*; Centers for Disease Control and Prevention: 2019.
33. Isabella, V. M.; Campbell, A. J.; Manchester, J.; Sylvester, M.; Nayar, A. S.; Ferguson, K. E.; Tommasi, R.; Miller, A. A., Toward the rational design of carbapenem uptake in pseudomonas aeruginosa. *Chemistry & biology* **2015,** *22*, 535-547.
34. Soundararajan, G.; Bhamidimarri, S. P.; Winterhalter, M., Understanding carbapenem translocation through occd3 (opdp) of pseudomonas aeruginosa. *Acs Chemical Biology* **2017,** *12*, 1656-1664.
35. Kohler, T.; Michea-Hamzehpour, M.; Epp, S. F.; Pechere, J. C., Carbapenem activities against pseudomonas aeruginosa: Respective contributions of oprd and efflux systems. *Antimicrobial Agents and Chemotherapy* **1999,** *43*, 424-427.
36. El Amin, N.; Giske, C. G.; Jalal, S.; Keijser, B.; Kronvall, G.; Wretlind, B., Carbapenem resistance mechanisms in pseudomonas aeruginosa: Alterations of porin oprd and efflux proteins do not fully explain resistance patterns observed in clinical isolates. *Apmis* **2005,** *113*, 187-196.
37. Tamber, S.; Ochs, M. M.; Hancock, R. E. W., Role of the novel oprd family of porins in nutrient uptake in pseudomonas aeruginosa. *Journal of Bacteriology* **2006,** *188*, 45-54.
38. Biswas, S.; Mohammad, M. M.; Patel, D. R.; Movileanu, L.; van den Berg, B., Structural insight into oprd substrate specificity. *Nature Structural & Molecular Biology* **2007,** *14*, 1108-1109.
39. Eren, E.; Vijayaraghavan, J.; Liu, J.; Cheneke, B. R.; Touw, D. S.; Lepore, B. W.; Indic, M.; Movileanu, L.; van den Berg, B., Substrate specificity within a family of outer membrane carboxylate channels. *PLoS biology* **2012,** *10*, e1001242.
40. Bonfiglio, G.; Russo, G.; Nicoletti, G., Recent developments in carbapenems. *Expert Opinion on Investigational Drugs* **2002,** *11*, 529-544.
41. Shah, P. M.; Isaacs, R. D., Ertapenem, the first of a new group of carbapenems. *Journal of Antimicrobial Chemotherapy* **2003,** *52*, 538-542.
42. Zhanel, G. G.; Wiebe, R.; Dilay, L.; Thomson, K.; Rubinstein, E.; Hoban, D. J.; Noreddin, A. M.; Karlowsky, J. A., Comparative review of the carbapenems. *Drugs* **2007,** *67*, 1027-1052.
43. Nicolau, D. P., Carbapenems: A potent class of antibiotics. *Expert Opinion on Pharmacotherapy* **2008,** *9*, 23-37.
44. Papp-Wallace, K. M.; Endimiani, A.; Taracila, M. A.; Bonomo, R. A., Carbapenems: Past, present, and future. *Antimicrobial Agents and Chemotherapy* **2011,** *55*, 4943-4960.
45. Torrie, G. M.; Valleau, J. P., Nonphysical sampling distributions in monte carlo free-energy estimation: Umbrella sampling. *Journal of Computational Physics* **1977,** *23*, 187-199.

46. Marrink, S. J.; Risselada, H. J.; Yefimov, S.; Tieleman, D. P.; de Vries, A. H., The martini force field: Coarse grained model for biomolecular simulations. *Journal of Physical Chemistry B* **2007,** *111*, 7812-7824.
47. Lopez, C. A.; Rzepiela, A. J.; de Vries, A. H.; Dijkhuizen, L.; Hunenberger, P. H.; Marrink, S. J., Martini coarse-grained force field: Extension to carbohydrates. *Journal of Chemical Theory and Computation* **2009,** *5*, 3195-3210.
48. Periole, X.; Cavalli, M.; Marrink, S. J.; Ceruso, M. A., Combining an elastic network with a coarse-grained molecular force field: Structure, dynamics, and intermolecular recognition. *Journal of Chemical Theory and Computation* **2009,** *5*, 2531-2543.
49. de Jong, D. H.; Singh, G.; Bennett, W. F. D.; Arnarez, C.; Wassenaar, T. A.; Schafer, L. V.; Periole, X.; Tieleman, D. P.; Marrink, S. J., Improved parameters for the martini coarse-grained protein force field. *Journal of Chemical Theory and Computation* **2013,** *9*, 687-697.
50. Marrink, S. J.; Tieleman, D. P., Perspective on the martini model. *Chemical Society Reviews* **2013,** *42*, 6801-6822.
51. Wassenaar, T. A.; Pluhackova, K.; Bockmann, R. A.; Marrink, S. J.; Tieleman, D. P., Going backward: A flexible geometric approach to reverse transformation from coarse grained to atomistic models. *Journal of Chemical Theory and Computation* **2014,** *10*, 676-690.
52. Ma, H. L.; Irudayanathan, F. J.; Jiang, W. J.; Nangia, S., Simulating gram-negative bacterial outer membrane: A coarse grain model. *Journal of Physical Chemistry B* **2015,** *119*, 14668-14682.
53. Ma, H. L.; Cummins, D. D.; Edelstein, N. B.; Gomez, J.; Khan, A.; Llewellyn, M. D.; Picudella, T.; Willsey, S. R.; Nangia, S., Modeling diversity in structures of bacterial outer membrane lipids. *Journal of Chemical Theory and Computation* **2017,** *13*, 811-824.
54. Graham, J. A.; Essex, J. W.; Khalid, S., Pycgtool: Automated generation of coarse-grained molecular dynamics models from atomistic trajectories. *Journal of Chemical Information and Modeling* **2017,** *57*, 650-656.
55. Abraham, M. J.; Murtola, T.; Schulz, R.; Páll, S.; Smith, J. C.; Hess, B.; Lindahl, E., Gromacs: High performance molecular simulations through multi-level parallelism from laptops to supercomputers. *SoftwareX* **2015,** *1-2*, 19-25.
56. Krieger, E.; Vriend, G., New ways to boost molecular dynamics simulations. *Journal of computational chemistry* **2015,** *36*, 996-1007.
57. Waterhouse, A.; Bertoni, M.; Bienert, S.; Studer, G.; Tauriello, G.; Gumienny, R.; Heer, F. T.; de Beer, T. A P.; Rempfer, C.; Bordoli, L.; Lepore, R.; Schwede, T., Swiss-model: Homology modelling of protein structures and complexes. *Nucleic Acids Research* **2018,** *46*, W296-W303.
58. Jo, S.; Kim, T.; Iyer, V. G.; Im, W., Charmm-gui: A web-based graphical user interface for charmm. *Journal of computational chemistry* **2008,** *29*, 1859-1865.
59. Wassenaar, T. A.; Ingólfsson, H. I.; Böckmann, R. A.; Tieleman, D. P.; Marrink, S. J., Computational lipidomics with insane: A versatile tool for generating custom membranes for molecular simulations. *Journal of Chemical Theory and Computation* **2015,** *11*, 2144-2155.
60. Vanommeslaeghe, K.; Hatcher, E.; Acharya, C.; Kundu, S.; Zhong, S.; Shim, J.; Darian, E.; Guvench, O.; Lopes, P.; Vorobyov, I.; Mackerell Jr, A. D., Charmm general force field: A force field for drug-like molecules compatible with the charmm all-atom additive biological force fields. *Journal of computational chemistry* **2010,** *31*, 671-690.
61. Berendsen, H. J. C.; Postma, J. P. M.; van Gunsteren, W. F.; DiNola, A.; Haak, J. R., Molecular dynamics with coupling to an external bath. *The Journal of chemical physics* **1984,** *81*, 3684-3690.
62. Pavelka, A.; Sebestova, E.; Kozlikova, B.; Brezovsky, J.; Sochor, J.; Damborsky, J., Caver: Algorithms for analyzing dynamics of tunnels in macromolecules. *IEEE/ACM transactions on computational biology and bioinformatics* **2016,** *13*, 505-17.
63. Humphrey, W.; Dalke, A.; Schulten, K., Vmd: Visual molecular dynamics. *Journal of Molecular Graphics* **1996,** *14*, 33-38.
64. The pymol molecular graphics system, version 2.0 Schrödinger, LLC.